JEM

Supplemental material

Lau et al., https://doi.org/10.1084/jem.20172323

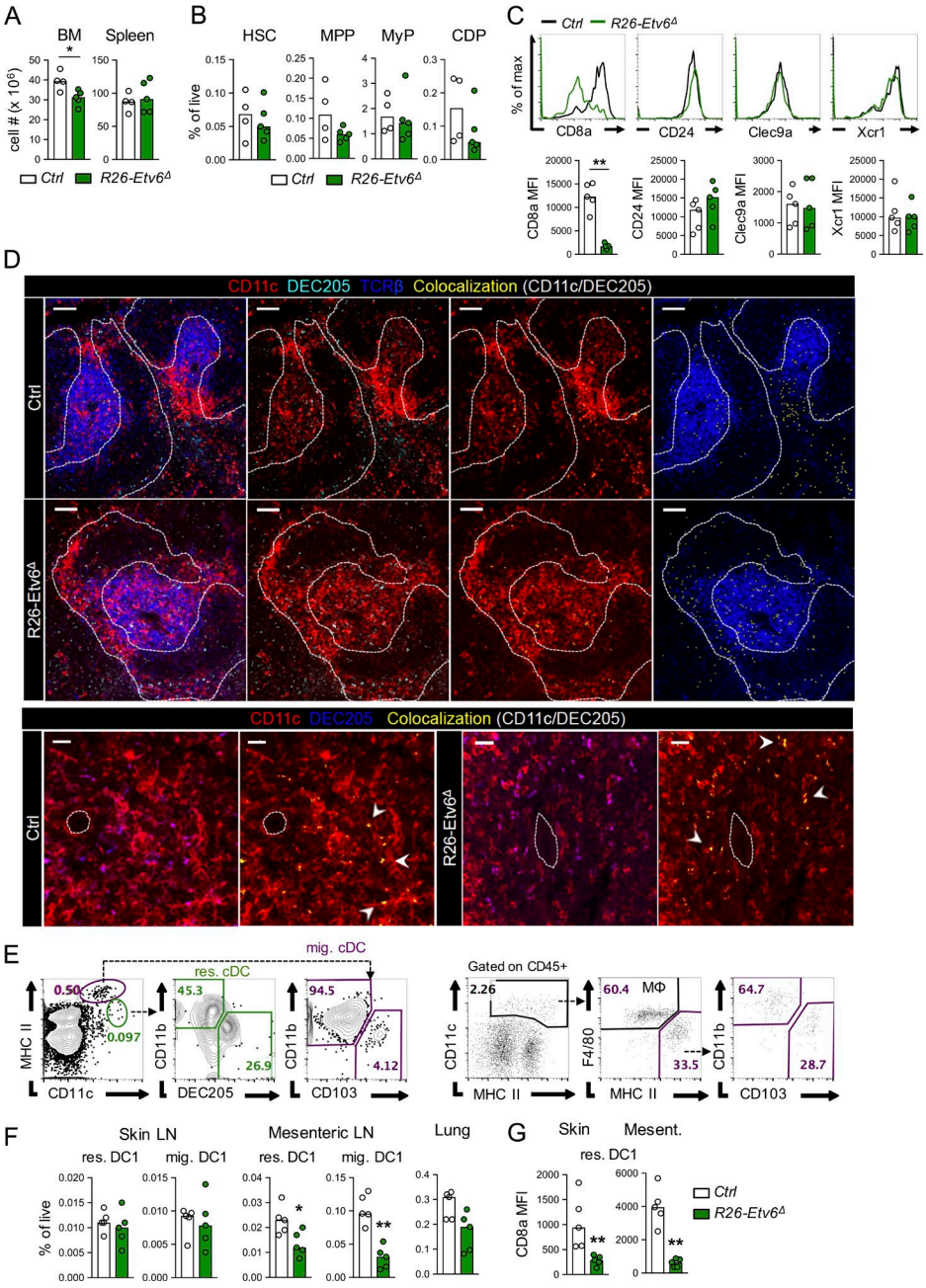

Figure S1. **Effect of Etv6 deletion on DC differentiation in vivo. (A)** Total cellularity of the BM and spleens of control and *R26-Etv6*$^{\Delta}$ animals 9 d after tamoxifen administration. Bars indicate the median of individual mice (n = 4–5) pooled from two experiments. Statistical significance by Mann–Whitney test (*, P ≤ 0.05). **(B)** Stem and progenitor cells in the BM of control and *R26-Etv6*$^{\Delta}$ animals 9 d after tamoxifen administration. Shown are the frequencies among total live BM cells of hematopoietic stem cells (HSCs; Lin$^-$ Sca-1$^+$ c-Kit$^+$ Flt3$^-$) multipotent progenitors (MPPs; Lin$^-$ Sca-1$^+$ c-Kit$^+$ Flt3$^+$), myeloid progenitors (MyPs; Lin$^-$ Sca-1$^-$ cKit$^+$), and CDPs (Lin$^-$ c-Kit^{lo} IL7R$^-$ Flt3$^+$ CD115$^+$). Bars indicate the median of individual mice (n = 4–5) pooled from two experiments. **(C)** The expression of DC1 markers in control and *R26-Etv6*$^{\Delta}$ animals 9 d after tamoxifen administration. Shown are representative histograms and MFI of CD8α, CD24, Clec9a, and Xcr1 on the splenic cDC1 population gated as shown in Fig. 2 C. Bars represent the median of individual mice (n = 5) pooled from two experiments. Statistical significance by Mann–Whitney test (**, P ≤ 0.01). **(D)** Confocal images of spleen sections from control and *R26-Etv6*$^{\Delta}$ animals 9 d after tamoxifen administration. Top: Staining for CD11c (red), DEC205 (cyan) and TCRβ (blue). Colocalization of CD11c and Dec205 is depicted in yellow. White dotted lines indicate B cell follicles as defined by simultaneous staining for B220 (not shown). Scale bars, 80 µm. Bottom: Staining for CD11c (red) and DEC205 (blue); colocalization of CD11c and Dec205 is depicted in yellow. White dotted lines define the periarteriolar lymphoid sheaths within T cell zones of the white pulp. Arrowheads indicate cDC1 cells. Scale bars, 20 µm. Images are representative of five individual mice per genotype. **(E–G)** cDC populations in the mesenteric and skin dLNs and in the lungs of *R26-Etv6*$^{\Delta}$ and control mice 9 d after tamoxifen treatment. **(E)** Representative staining plots of showing CD11c^{hi} MHCII^{lo} lymphoid organ-resident and CD11c^{lo} MHCII^{hi} migratory cDCs in the lymph nodes (left panel) and CD11c$^+$ MHCII^{hi} F4/80^{lo} tissue-resident cDCs in the lung (right panel). Resident and migratory cDC1 were defined as CD11b$^-$ Dec205$^+$ and CD11b$^-$ CD103$^+$, respectively. **(F)** The fractions of resident and migratory cDC1 in the LNs and of the tissue cDC1 in the lung. Bars represent the median of individual mice (n = 5) pooled from two experiments. Statistical significance by Mann–Whitney test (*, P ≤ 0.05; **, P ≤ 0.01). **(G)** Expression of CD8α on lymphoid organ-resident cDC1 in skin dLNs and mesenteric LNs. Bars represent the median MFI of individual mice (n = 5) pooled from two experiments. Statistical significance by Mann–Whitney test (**, P ≤ 0.01).

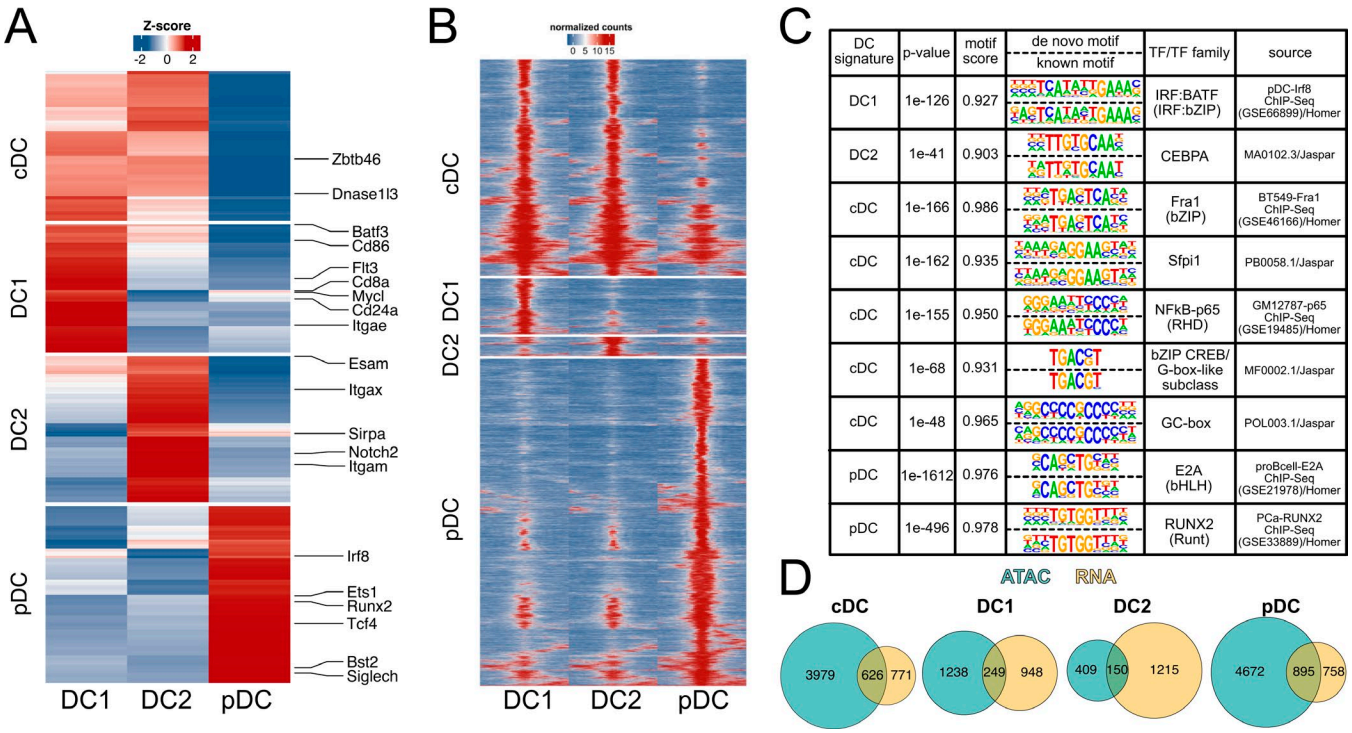

Figure S2. **DC subsets display distinct transcriptional and epigenetic signatures that are altered by Etv6 deficiency.** Primary splenic DC subsets (pDC, cDC1, Esam^{hi}, and Esam^{lo} cDC2) were sorted from individual chimeric mice reconstituted with BM from DC-*Etv6*$^{\Delta}$ (CKO) or control WT donors. The resulting cell populations were analyzed by RNA-seq or ATAC-seq; $n = 2$ per genotype. **(A)** Heatmap of transcriptional signatures of DC subsets derived from RNA-seq profiles of WT samples. Each row represents a gene; select genes with known specific expression in the respective DC subset are highlighted. **(B)** Heatmap of open chromatin signatures of DC subsets derived from ATAC-seq profiles of WT samples. Each row represents a peak; signal is displayed as normalized read counts over 2 kb centered at the peak region, and binned at 40-bp windows. **(C)** Transcription factor–binding motifs enriched in the chromatin signatures shown in panel B. De novo motif analysis was performed on peak regions within each chromatin signature as calculated using HOMER software. The motifs showing a motif score (similarity match) of >0.9 are depicted. **(D)** Venn diagrams show overlap of gene signatures defined by transcriptional (RNA-seq) and chromatin accessibility (ATAC-seq) profiles. Numbers in yellow circles represent genes defined within the respective RNA-seq signature. Numbers in cyan circles represent genes that had peaks assigned to them within the respective ATAC-seq signature.

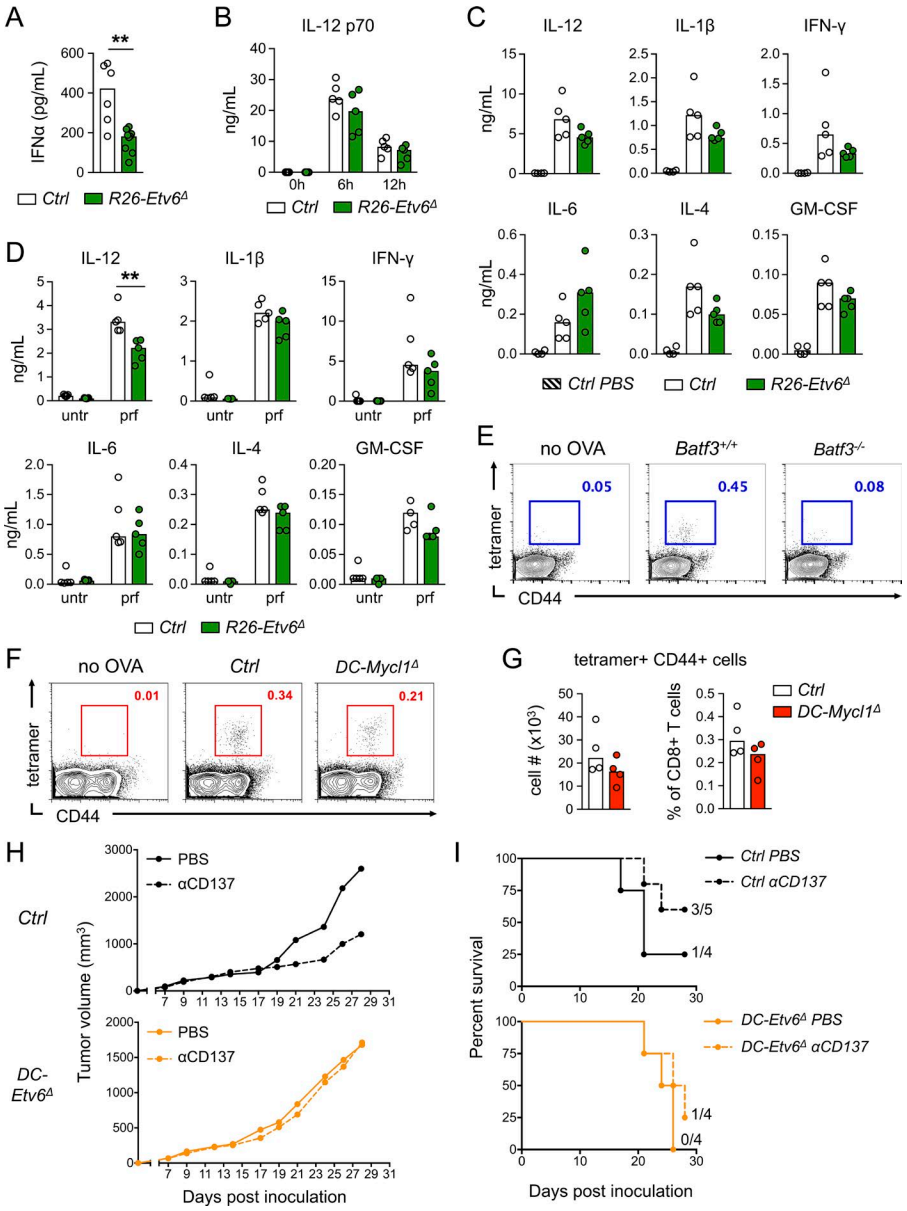

Figure S3. **Characterization of DC functions in vivo. (A)** TLR9-induced IFN-α production in vivo. Tamoxifen-induced *R26-Etv6*$^{\Delta}$ or control animals were injected i.v. with lipid-coated CpG-A, and serum was analyzed 6 h later. Shown is the concentration of IFN-α in the sera as determined by ELISA. Bars indicate the median of individual mice (n = 6–9) pooled from two experiments. Statistical significance by Mann–Whitney test (**, P ≤ 0.01). **(B and C)** Cytokine production in response to the *T. gondii* STAg in *R26-Etv6*$^{\Delta}$ and control mice 9 d after tamoxifen administration. **(B)** Mice were injected with 25 µg STAg, and the production IL-12 p70 in the sera was determined 6 and 12 h later by ELISA. Shown are individual values of n = 5 mice from a single experiment; bars represent the median. **(C)** Mice were injected with 20 µg STAg, and the production of IL-12, IL-1β, IFN-γ, IL-6, IL-4, and GM-CSF in the sera was determined 6 h later by Luminex multiplex assay. Shown are individual values of n = 4–5 mice pooled from two experiments; bars represent the median. Separate control mice were injected with PBS to determine baseline levels of each cytokine. **(D)** TLR11-induced cytokine production in vitro. Splenic DCs isolated from tamoxifen-induced *R26-Etv6*$^{\Delta}$ or control animals were stimulated with *T. gondii* profilin (prf) for 24 h. The levels of IL-12, IL-1β, IFN-γ, IL-6, IL-4, and GM-CSF in culture supernatants were determined by Luminex multiplex assay. Bars indicate the median of individual mice (n = 5) pooled from two experiments. Statistical significance by Mann–Whitney test (**, P ≤ 0.01). **(E)** cDC1-dependent in vivo cross-priming of antigen-specific CD8$^+$ T cells by allogeneic splenocytes. OVA-pulsed splenocytes from FVB mice (H-2^q) were injected i.v. into cDC1-deficient *Batf3*$^{-/-}$ mice or WT controls. 7 d after the transfer, the spleens were harvested and analyzed for OVA-specific CD8$^+$ T cells using OVA peptide/H-2K^b tetramer staining. Shown are representative staining plots with the fraction of tetramer-positive cells out of total CD8$^+$ T cells indicated. **(F and G)** Role of Mycl1 in cDC1-dependent in vivo cross-priming of antigen-specific CD8$^+$ T cells. The cross-priming assay in *DC-Mycl1*$^{\Delta}$ (*Mycl1*$^{flox/flox}$ *Itgax*-Cre$^+$) and control WT animals was performed as in panel E, except that BALB/c (H-2^d) splenocytes were used. Shown are representative staining plots with the fraction of tetramer-positive cells out of total CD8$^+$ T cells indicated (F) and absolute numbers of tetramer-positive cells and frequencies of tetramer-positive cells among total CD8$^+$ T cells in the spleen (G). Bars represent the median of individual values (n = 4) from a single experiment**. (H and I)** Response to antitumor therapy with immunomodulatory antibodies. DC-*Etv6*$^{\Delta}$ (*Etv6*$^{flox/-}$ *Itgax*-Cre) or control (*Etv6*$^{flox/flox}$) animals were inoculated with MC38 adenocarcinoma cells and treated with anti-CD137 or vehicle (PBS) on days 4, 7, and 10 after inoculation. **(H)** Tumor growth plots. Shown are median tumor volumes at the indicated time points (n = 4–5) from a single experiment. **(I)** Survival curves. Shown are the fractions of animals (n = 4–5 from a single experiment) that did not reach an endpoint defined as a tumor volume >2,000 mm^3 or visible wounding.

Tables S1–S9 are provided as Excel files. Table S1 shows gene expression in control and Etv6-deficient splenic cDC1 (Dec205$^+$) as determined by RNA-seq. Listed are normalized gene counts in each replicate sample from CKO or WT mice, the average of the normalized counts taken over all samples (baseMean), $\log_2$-transformed difference between WT and CKO (log2FC) and its standard error (lfcSE), Wald statistics (stat) and Wald test P value (P value), padj, and Boolean values of IRF8 targets that are upregulated (irf8.up) or downregulated (irf8.down) upon IRF8 deficiency. Genes are listed by increasing padj value.

Table S2 shows gene expression in control and Etv6-deficient splenic cDC2 (Esam^{hi}) as determined by RNA-seq. Listed are normalized gene counts in each replicate sample from CKO or WT mice, the average of the normalized counts taken over all samples (baseMean), $\log_2$-transformed difference between WT and CKO ($\log_2$FC) and its standard error (lfcSE), Wald statistics (stat) and Wald test P value (P value), padj, and Boolean values of IRF8 targets that are upregulated (irf8.up) or downregulated (irf8.down) upon IRF8 deficiency. Genes are listed by increasing padj value.

Table S3 shows gene expression in control and Etv6-deficient splenic cDC2 (Esam^{lo}) as determined by RNA-seq. Listed are normalized gene counts in each replicate sample from CKO or WT mice, the average of the normalized counts taken over all samples (baseMean), $\log_2$-transformed difference between WT and CKO (log2FC) and its standard error (lfcSE), Wald statistics (stat) and Wald test P value (P value), padj, and Boolean values of IRF8 targets that are upregulated (irf8.up) or downregulated (irf8.down) upon IRF8 deficiency. Genes are listed by increasing padj value.

Table S4 shows gene expression in control and Etv6-deficient splenic pDCs as determined by RNA-seq. Listed are normalized gene counts in each replicate sample from CKO or WT mice, the average of the normalized counts taken over all samples (baseMean), $\log_2$-transformed difference between WT and CKO ($\log_2$FC) and its standard error (lfcSE), Wald statistics (stat) and Wald test P value (P value), padj, and Boolean values of IRF8 targets that are upregulated (irf8.up) or downregulated (irf8.down) upon IRF8 deficiency. Genes are listed by increasing padj value.

Table S5 shows gene expression signatures of splenic DC subsets. Listed are genes and their assignments to the RNA-seq signatures (RNA_DC_Sig); genes not belonging to subset signatures are indicated as "other".

Table S6 shows open chromatin peaks in control and Etv6-deficient splenic cDC1 (Dec205$^+$) as determined by ATAC-seq. Listed are normalized peak counts in each replicate sample from CKO or WT mice; peak genomic coordinates, type, and gene assignment; and the differential expression statistics described above for Tables S1, S2, S3, and S4. Peaks are listed by increasing padj value.

Table S7 shows open chromatin peaks in control and Etv6-deficient splenic pDCs as determined by ATAC-seq. Listed are normalized peak counts in each replicate sample from CKO or WT mice; peak genomic coordinates, type, and gene assignment; and the differential expression statistics described above for Tables S1, S2, S3, and S4. Peaks are listed by increasing padj value.

Table S8 shows open chromatin peaks in control and Etv6-deficient splenic cDC2 as determined by ATAC-seq. Listed are normalized peak counts in each replicate sample from CKO or WT mice; peak genomic coordinates, type, and gene assignment; and the differential expression statistics described above for Tables S1, S2, S3, and S4. Peaks are listed by increasing padj value.

Table S9 shows open chromatin signatures of splenic DC subsets. Listed are ATAC-seq peaks with genomic coordinates, type, and gene assignment; chromatin signature assignments of peaks (ATAC_DC_Sig) and transcriptional signature assignments of the corresponding genes (RNA_DC_Sig); and binding by IRF8 in the culture-derived cDC1 or pDCs (1 for binding, 0 for no binding). Peaks and/or genes not belonging to subset signatures are indicated as "other."